Kinetic event-chain algorithm for active matter

Nico Schaffrath, Thevashangar Sathiyanesan, Tobias A. Kampmann, and Jan Kierfeld*
Physics Department, TU Dortmund University, 44221 Dortmund, Germany

(Received 18 October 2021; accepted 3 May 2026; published 5 June 2026)

We present a cluster kinetic Monte Carlo algorithm for active matter systems of self-propelled particles with special focus on steric interactions. The kinetic event-chain algorithm is based on the event-chain Monte Carlo method and is applied to active Brownian disks in two dimensions. The algorithm assigns Monte Carlo moves of active disks a mean time based on a comparison between Brownian dynamics and the dynamics of the event-chain Monte Carlo method. This time is used to perform diffusional rotation of their propulsion force. We show that the algorithm correctly and efficiently reproduces various physical results ranging from single-particle dynamics to many-body effects. In particular, we reproduce the phase diagram of active disks and the motility-induced phase-separated region with high accuracy. The kinetic event-chain algorithm is shown to be much faster—at comparable accuracy—than (event-driven) Brownian dynamics algorithms, enabling large-scale simulations up to giant systems with 10^5 particles on standard desktop hardware.

DOI: 10.1103/hhbb-ph5s

I. INTRODUCTION

Active matter systems are nonequilibrium many-particle systems that are driven by a propulsion force at the level of individual particles. This gives rise to continuous energy dissipation, local time-reversal symmetry breaking, and entropy production [1]. Active matter can be found at all length scales for both synthetic and biological systems [2]; examples comprise self-propelled colloidal particles [3] and microswimmers [4], cytoskeletal filaments propelled by molecular motors [5–7], colonies of bacteria [8], and swarms of animals [9].

In the simplest active systems, the propulsion force direction is anchored to the individual particle, which breaks the rotational symmetry at the particle level. The force changes direction upon diffusive reorientation of the particle. The propulsion energy sets particles in motion and is dissipated via a surrounding bath, which breaks detailed balance and gives rise to nonequilibrium physics. The most popular theoretical and numerical models are active Brownian particles (ABPs) with an overdamped motion and a heat bath modeled by Brownian random forces (Langevin dynamics).

Interacting active matter exhibits collective phenomena, which are not present in the corresponding equilibrium systems. One prominent example is the motility-induced phase separation (MIPS) of self-propelled hard spheres or disks [10,11], which is an activity-driven clustering phenomenon driven by the active blocking of particles with opposing propulsion directions. More complicated phase behavior occurs for nonspherical particles or in the presence of alignment interactions [2].

Despite considerable progress during the last decade [12], simulation methods for active many-particle systems are largely limited to Langevin or molecular dynamics techniques. While Monte Carlo (MC) algorithms produced much of the numerical progress in statistical physics of equilibrium phase transitions, the development of kinetic MC schemes for active matter started only recently [13–16]. Moreover, cluster MC algorithms have not been proposed at all for active systems so far, while rejection-free cluster MC algorithms have proven to be a powerful tool for lattice spin systems [17,18] and—as event-chain (EC) MC [19]—also for off-lattice simulations of many-particle systems.

In this paper, we present the first cluster kinetic MC scheme for the simulation of active matter systems of self-propelled particles, with main focus on steric interactions, i.e., genuinely hard particles. The algorithm is a kinetic event-chain (kEC) algorithm based on the ECMC method. A dense system of ABPs with exemplary MC cluster moves is depicted in Fig. 1. Throughout this work, we use OVITO [20] to visualize configurations of interest. The algorithm becomes exact in the limit of small EC lengths, i.e., small MC cluster moves, and is applied to systems of genuinely hard active disks and active Lennard-Jones disks in two dimensions. It is important to note that standard Brownian dynamics simulations cannot be applied to hard active particles. We verify the kEC algorithm by analyzing multiple observables in these systems, particularly focusing on the phase diagram of active hard disks and mapping out the MIPS region. For Lennard-Jones disks, we can compare to Brownian dynamics simulations performed using the LAMMPS package [21], with respect to accuracy. For hard disks, we can benchmark and compare to a version of the event-driven Brownian-dynamics (EDBD) algorithm [22], which takes the self-propulsion of ABPs into account [23] and was used by Levis *et al.* [24] to investigate the system's MIPS region.

*Contact author: jan.kierfeld@tu-dortmund.de

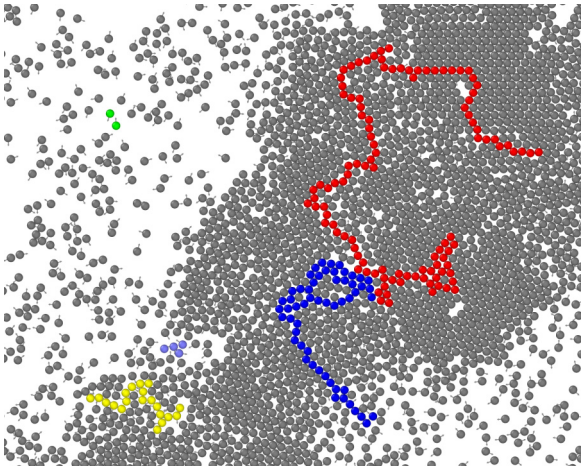

FIG. 1. Exemplary snapshot of a system of hard ABPs where MIPS occurs. To each particle a small arrow is anchored, representing the current direction of the active force. The particles that participated in the last five cluster moves are highlighted using colors. The higher the local packing fraction, the more particles are displaced in a typical cluster move.

II. KINETIC EVENT-CHAIN MONTE CARLO ALGORITHM

EC algorithms are a variant of irreversible Markov-Chain MC algorithms [25] and have been applied to a wide range of systems in the last decade [19,26–32]. They can also be classified as cluster algorithms. We focus on steric interactions to introduce the concepts of the algorithm in the following. In a hard-disk system, an EC cluster is constructed by choosing a random unit direction $\boldsymbol{e}_{\mathrm{EC}}$ and a random initial disk. Starting with the initial disk, the "moving" disk is displaced in direction $\boldsymbol{e}_{\mathrm{EC}}$ until collision with another disk. In a billiardlike fashion, the hit disk becomes the "moving" disk (in a so-called *lifting move*) and is displaced in direction $\boldsymbol{e}_{\mathrm{EC}}$ until the next collision. The cluster move ends if the total displacement equals a prescribed EC length ℓ_{EC}, which is a parameter of the EC algorithm. The resulting cluster moves of chains of particles are rejection-free and satisfy global balance rather than detailed balance [19,27]. Compared to local Metropolis-Hastings MC [33], speedups of up to 2 orders of magnitude can be achieved [19,28,31].

MC algorithms are not based on an equation of motion and, thus, lack a proper definition of time. ABPs, on the other hand, are described by explicitly time-dependent Brownian dynamics. A system of N active particles (particle index i) in two dimensions, which are driven with propulsion force F_0 in the unit directions $\boldsymbol{e}_i(t) = (\cos(\theta_i), \sin(\theta_i))$, is described by

$$\dot{\boldsymbol{r}}_i(t) = v_0 \boldsymbol{e}_i(t) + \boldsymbol{\xi}_i(t) + \boldsymbol{f}_i(t), \tag{1}$$

where $\boldsymbol{r}_i(t)$ are the particle positions. Here, $v_0 = F_0/\Gamma$ is the driving velocity for a friction constant Γ, and $\boldsymbol{\xi}_i(t)$ is a Gaussian thermal noise with zero mean and correlations $\langle \boldsymbol{\xi}_i(t) \boldsymbol{\xi}_j^T(t') \rangle = 2D\mathbf{1}\delta_{ij}\delta(t-t')$, where $D = k_B T/\Gamma$ is the translational diffusion constant. The remaining active particles exert interaction forces $\boldsymbol{f}_i = \boldsymbol{F}_i/\Gamma$; we focus on monodisperse systems with particle diameter σ. The propulsion direction $\boldsymbol{e}_i(t)$ undergoes free rotational diffusion, i.e.,

$$\langle \dot{\theta}_i(t) \dot{\theta}_j(t') \rangle = 2D_r \delta_{ij} \delta(t-t'), \tag{2}$$

with the rotational diffusion constant $D_r = 3D/\sigma^2$ (for hydrodynamic reasons [24]). The activity of a single ABP is characterized by the dimensionless Péclet number

$$\mathrm{Pe} \equiv \frac{v_0}{\sigma D_r}. \tag{3}$$

Individual active particles perform persistent random walks with a persistence time $\tau = 1/D_r$ because the propulsion force direction undergoes rotational diffusion. Equilibrium MC algorithms lack this persistent motion because of their Markovian nature. Several kinetic MC schemes have been proposed for active particles [13–16], where a temporal correlation of MC particle moves has been introduced to establish persistence. In conjunction with Metropolis sampling of interactions, these kinetic MC schemes show nonequilibrium phenomena like MIPS for repulsive active particles. For example, the algorithm developed by Klamser *et al.* [16] advances time in equidistant time steps Δt and the direction $\boldsymbol{e}_i$ is updated by a small random rotation ensuring the proper persistence. Regarding the spatial displacement, the authors showed, both numerically and analytically, that their method becomes ill-defined in the limit of small time steps Δt if active particle displacements rely purely on persistent steps. To restore correct dynamics, a blended algorithm was introduced, which mixes steps in random directions with the persistent ones. For the blended algorithm, an exact mapping to ABPs can be established, as the authors subsequently showed their method leads to the same Fokker-Planck equation in the limit of small time steps Δt as Brownian dynamics.

The very basic idea of our kEC algorithm, in order to simulate ABPs, is to use the standard ECMC method to generate moves, based on the rules for passive equilibrium systems, and afterward update the direction of the active force using a newly introduced mean time per move. This way, we want to achieve an algorithm that is as effective as ECMC simulations for hard spheres, while it can correctly deal with the dynamic situation of active particles.

With this in mind, we view each active particle as a particle under its individual constant force $F_0\boldsymbol{e}$ and, thus, in its individual constant linear potential over the course of each ECMC move. We then calculate the mean move length in force direction $\langle \Delta \boldsymbol{r}_{\mathrm{EC}} \cdot \boldsymbol{e} \rangle$ of a single particle per ECMC move (see below for the analytical calculation). Because $\langle \Delta \boldsymbol{r} \cdot \boldsymbol{e} \rangle = v_0 \Delta t$ holds for a single ABP exactly, we identify $\langle \Delta t_{\mathrm{EC}} \rangle = \langle \Delta \boldsymbol{r}_{\mathrm{EC}} \cdot \boldsymbol{e} \rangle / v_0$. By assigning $\langle \Delta t_{\mathrm{EC}} \rangle$ to pass for each ECMC move, we are able to introduce an exact mean time into our algorithm. It amounts to a dynamical mean-field assumption, because we apply a mapping between kEC time and ABP time that has been derived from the mean time for an ECMC displacement move. Because we also find $\langle \Delta \boldsymbol{r}_{\mathrm{EC}} \cdot \boldsymbol{e} \rangle = \langle \Delta \boldsymbol{r}_{\mathrm{EC}} \rangle \cdot \boldsymbol{e}$ for the ECMC algorithm, we obtain the identical time assignment rule based on the mean displacement vector $\langle \Delta \boldsymbol{r}_{\mathrm{EC}} \rangle$ per ECMC move. This will be important later on to derive that the kEC algorithm becomes exact in the limit of small EC lengths. Using the assigned time $\langle \Delta t_{\mathrm{EC}} \rangle$, we readjust the force direction according to rotational diffusion after each ECMC move.

For the analytical calculation of the mean move length in force direction $\langle \Delta \boldsymbol{r}_{\rm EC} \cdot \boldsymbol{e} \rangle$, it is sufficient to consider a single active particle under a constant force $F_0\boldsymbol{e}$ or in a corresponding linear potential $V(\boldsymbol{r})$. In an external potential, the ECMC algorithm works as follows [26,30,32]: A random EC direction $\boldsymbol{e}_{\rm EC}$ is chosen. If the move is energetically downhill ($\cos\phi \equiv \boldsymbol{e}_{\rm EC} \cdot \boldsymbol{e} \geqslant 0$), the particle is displaced by the full EC length, $\Delta \boldsymbol{r} = \ell_{\rm EC}\boldsymbol{e}_{\rm EC}$. If the move is energetically uphill ($\cos\phi < 0$), a "usable" energy $\Delta U > 0$ is drawn from a Boltzmann distribution $p(\Delta U) \sim \exp(-\beta \Delta U)$ (with $\beta = 1/k_B T$), and a rejection distance $d_{\rm rej}$ is determined from $\Delta U = -F_0 d_{\rm rej} \cos\phi$. If $d_{\rm rej} \geqslant \ell_{\rm EC}$, the particle is moved by the full EC length, $\Delta \boldsymbol{r} = \ell_{\rm EC}\boldsymbol{e}_{\rm EC}$. If $d_{\rm rej} < \ell_{\rm EC}$, the particle is only moved by $\Delta \boldsymbol{r} = d_{\rm rej}\boldsymbol{e}_{\rm EC}$, the EC direction is lifted $\boldsymbol{e}_{\rm EC} \to \boldsymbol{e}'_{\rm EC}$ (by reflecting with respect to the equipotential surface, i.e., $\boldsymbol{e}'_{\rm EC} = \boldsymbol{e}_{\rm EC} - 2\cos\phi \boldsymbol{e}$), and the particle is moved by the remaining EC length $\ell_{\rm EC} - d_{\rm rej}$ in the new downhill direction. In total, this results in $\Delta \boldsymbol{r} = d_{\rm rej}\boldsymbol{e}_{\rm EC} + (\ell_{\rm EC} - d_{\rm rej})\boldsymbol{e}'_{\rm EC}$. After this EC move, a new direction $\boldsymbol{e}_{\rm EC}$ is chosen, and we start over. Averaging over all cases and all randomly chosen EC directions $\boldsymbol{e}_{\rm EC}$ (angles ϕ), we obtain

$$\frac{\langle \Delta \boldsymbol{r}_{\rm EC} \cdot \boldsymbol{e} \rangle}{\ell_{\rm EC}} = x f(x),$$

with a dimensionless parameter

$$x \equiv \beta F_0 \ell_{\rm EC} = v_0 \ell_{\rm EC}/D = 3{\rm Pe}\ell_{\rm EC}/\sigma \tag{4}$$

and a scaling function

$$f(x) = \frac{2}{\pi}\frac{1}{x} - \frac{1}{x^2}\frac{1}{\pi}\int_{-\pi/2}^{\pi/2} d\phi (1 - e^{-x\cos\phi}), \tag{5}$$

which is monotonically decreasing with asymptotics $f(x) \approx 1/4$ for $x \ll 1$ and $f(x) \approx 2/\pi x$ for $x \gg 1$, (see Sec. I B of the Supplemental Material [34]).

For the ECMC move mean time $\langle \Delta t_{\rm EC} \rangle = \langle \Delta \boldsymbol{r}_{\rm EC} \cdot \boldsymbol{e} \rangle / v_0$, we use $\ell_{\rm EC}/v_0 = \tau x/3{\rm Pe}^2$ and obtain

$$\langle \Delta t_{\rm EC} \rangle = \tau \frac{1}{3{\rm Pe}^2} x^2 f(x), \tag{6}$$

such that $\langle \Delta t_{\rm EC} \rangle$ only depends on the active force F_0 and the EC length $\ell_{\rm EC}$ via Pe and x. For weak active drive or small EC lengths $x \ll 1$, we get $\langle \Delta t_{\rm EC} \rangle \approx \ell_{\rm EC}^2/4D$ reminiscent of a diffusive timescale. The opposite limit of strong active drive or large EC lengths $x \gg 1$ leads to $\langle \Delta t_{\rm EC} \rangle \approx 2\ell_{\rm EC}/\pi v_0$ reminiscent of a timescale for directed motion.

In the simulation, after each ECMC move, the force direction is updated $\theta' = \theta + \Delta\theta$ by drawing an angle $\Delta\theta$ from a Gaussian distribution using $\mu_\theta = \theta$ and $\sigma_\theta = \sqrt{2D_r \langle \Delta t_{\rm EC} \rangle}$. For a single active particle, this is only a good approximation if updates remain smooth, $\langle \Delta t_{\rm EC} \rangle \ll \tau$. From Eq. (6), we can show this is equivalent to $x \ll (3\pi/2){\rm Pe}^2$ or to require moderately small EC lengths $\ell_{\rm EC}/\sigma \ll (\pi/2){\rm Pe}$ for high activity ${\rm Pe} > 1$ (and $x \ll 2\sqrt{3}{\rm Pe}$ or $\ell_{\rm EC}/\sigma \ll 2/\sqrt{3}$ in the passive limit ${\rm Pe} \ll 1$).

In the many-particle system, we combine the ECMC procedure for one active particle with the hard-disk collision ECMC rules outlined above. Then, we simulate a Hamiltonian $\mathcal{H} = \sum_i [-F_0 \boldsymbol{e}_i \cdot \boldsymbol{r}_i + V_i(\{\boldsymbol{r}_i\})]$, where the driving forces $F_0\boldsymbol{e}_i$ enter as individual external linear potentials, with the usual ECMC scheme assuming fixed $\boldsymbol{e}_i$ during each EC move.

This results, as a consequence of the previously mentioned *lifting moves*, in ECs with more than one participating particle. The purpose of lifting is to avoid MC rejections caused by collisions by lifting the event chain to the collision partner and continuing the MC motion. As a result, in each EC, we move particles by the same total distance $\ell_{\rm EC}$ as in a single-particle system, but distribute the total distance to all particles i in the EC, which move a distance Δd_i with $\sum_{i\in{\rm EC}} \Delta d_i = \ell_{\rm EC}$. In order to assign a proper time to each moving particle i in the EC, we distribute the mean time $\langle \Delta t_{\rm EC} \rangle$ of a single-particle EC move without collisions over all particles i in the EC according to their displacements Δd_i. Since collisions are instantaneous in case of hard disks, this leads to

$$\langle \Delta t_{\rm EC} \rangle_i = \frac{\Delta d_i}{\ell_{\rm EC}} \langle \Delta t_{\rm EC} \rangle. \tag{7}$$

After each EC, the force directions of all participating particles i are updated by drawing $\Delta\theta_i$ from Gaussian distributions with mean $\mu_{\theta_i} = \theta_i$ and variance $\sigma^2_{\theta_i} = 2D_r \langle \Delta t_{\rm EC} \rangle_i$. The assignment of individual times $\langle \Delta t_{\rm EC} \rangle_i$ leads to each particle having its "own simulation time."

The choice (7) for the time $\langle \Delta t_{\rm EC} \rangle_i$ proportional to its moving distance Δd_i in the EC is the only choice that ensures a *constant* algorithmic particle velocity $v_i = \Delta d_i / \langle \Delta t_{\rm EC} \rangle_i$ (regarding collisions and subsequent lifting event to be instantaneous) and, thus, a uniform particle current along an EC. Within each EC, global balance is satisfied by construction of the algorithm. If ECs are started where the previous EC ended, this results in strict global balance. This means that the N-particle probability current density in configurational space is divergence-free. Starting ECs where the previous EC ended can produce artifacts in the distribution of the individual particle simulation times, because (1) particles in dense regions tend to be updated not only proportional to density, but more frequently and (2) spatially inhomogeneities of this distribution are amplified.

Therefore, we start new ECs at randomly chosen particles but the algorithm should retain divergence-free probability current densities on average. With the choice (7) translating configurational moves into moves with constant velocity, this leads to a divergence-free N-particle current density. This is, however, exactly the condition for a dynamic stationary state in a nonequilibrium system such as active disks [35]. Therefore, the choice (7) is the unique choice that is compatible with a dynamic stationary state in the active system. In Eq. (7), we also use the single-particle EC move time $\langle \Delta t_{\rm EC} \rangle$ in the absence of collisions to be distributed over the over all particles i. This guarantees correct currents in *dilute* regions of a system, where particles are essentially isolated. Ensuring constant currents along ECs that can cross the entire system by using Eq. (7) then correctly establishes the necessary current equilibrium between dense and dilute regions of the system. Loosely speaking, Eq. (7) enforces the kEC currents to be divergence-free and constant along an EC via global balance, and the size of the currents generated by the kEC algorithm is gauged to be correct in the dilute regions.

As stated above, the assignment of individual times $\langle \Delta t_{\rm EC} \rangle_i$ according to Eqs. (6) and (7) leads to each particle having its "own simulation time." Therefore, we have to make sure that each particle has essentially the same simulation

time, i.e., that the distribution of particle simulation times is sufficiently narrow. We confirmed that the relative standard deviation $\sigma_{\Delta t}/\mu_{\Delta t}$ of the resulting distribution of simulation times Δt decreases continuously by increasing the mean simulation time $\mu_{\Delta t}$ per particle or by decreasing the EC length, $\sigma_{\Delta t}/\mu_{\Delta t} = a(N)\ell_{\mathrm{EC}}^{\alpha}\mu_{\Delta t}^{-1/2}$, as detailed in the Supplemental Material [34]. This holds for different values of parameters, i.e., regardless of whether MIPS occurs. Therefore, the algorithm can be set up so that the simulation time is, on average, equal for all particles. A condition $\sigma_{\Delta t} < \tau$ will assure that particles remain within one persistence time; i.e., the propulsion directions will not be affected by the time spread. For $\ell_{\mathrm{EC}} = 0.01\sigma$, we can simulate for several thousand persistence times using the kEC algorithm without violating this criterion. Also, the above condition $\langle\Delta t_{\mathrm{EC}}\rangle D_r \ll 1$ for smooth rotations becomes much weaker in a many-particle system, as it only requires $\langle\Delta t_{\mathrm{EC}}\rangle_i D_r \ll 1$ and $\langle\Delta t_{\mathrm{EC}}\rangle_i \ll \langle\Delta t_{\mathrm{EC}}\rangle$. This is hardly ever a concern.

III. VALIDITY OF THE ALGORITHM

Our above arguments suggest that the kEC algorithm samples single active particles (the dilute limit) correctly on average and that it samples stationary dynamic states of many active particles correctly on average. This does not mean that the microscopic dynamics will be exact. The kEC algorithm can become potentially inexact because of the effective time dependence of the Hamiltonian: The external driving forces represent individual external linear potentials, but they change direction as a function of time by rotational diffusion. We handle this time dependence by introducing the mean time $\langle\Delta t_{\mathrm{EC}}\rangle$ per EC for a single ABP and redistributing this time properly over the particles participating in an EC for many ABPs. This procedure is only correct *on average*. However, there are two opposite limiting cases, where our algorithm becomes strictly exact: (1) in the passive limit $\mathrm{Pe} \to 0$, the driving potentials effectively vanish and (2) in the opposite limit $\mathrm{Pe} \to \infty$ of large Péclet numbers $\mathrm{Pe} \equiv v_0/(\sigma D_r)$ or $D_r \to 0$, the directions of the driving forces become essentially quenched. In both cases, the Hamiltonian becomes effectively time-independent, the correctness of the mean time $\langle\Delta t_{\mathrm{EC}}\rangle$ per EC irrelevant, and the kEC algorithm equivalent to a standard ECMC simulation.

The exactness for both $\mathrm{Pe} \to 0$ and $\mathrm{Pe} \to \infty$ already suggests that the kEC algorithm should stay accurate over a fairly large range of Péclet numbers and deviations for all intermediate Péclet numbers remain small. For intermediate Péclet numbers, the dimensionless parameter $x = \beta F_0 \ell_{\mathrm{EC}}$ from Eq. (4) plays a key role for the validity of our algorithm. This can be shown explicitly for a single ABP. We assign a kEC simulation time $\langle\Delta t_{\mathrm{EC}}\rangle$ to a single ABP using the *first* moment of the displacement in force direction $\langle\Delta \boldsymbol{r}\cdot\boldsymbol{e}\rangle = v_0\Delta t$ by requiring that $\langle\Delta \boldsymbol{r}_{\mathrm{EC}}\cdot\boldsymbol{e}\rangle = v_0\langle\Delta t_{\mathrm{EC}}\rangle$. As shown in the Sec. II of the Supplemental Material [34], we can also calculate *higher* moments related to the dynamics of a single free ABP, such as $\langle(\Delta \boldsymbol{r}_{\mathrm{EC}}\cdot\boldsymbol{e})^2\rangle$ and $\langle\Delta \boldsymbol{r}_{\mathrm{EC}}^2\rangle$, on a single-step level. However, these quantities only match their analytical counterparts from Brownian dynamics in the limit $x \to 0$. On the contrary, the larger x, the more does our algorithm's single-step behavior differ from actual Brownian dynamics of ABPs. More importantly, we derive a Fokker-Planck equation for the probability density $P_{\mathrm{kEC}}(\boldsymbol{r},\theta,t)$ to find a single particle at position $\boldsymbol{r}$ and force direction θ at times t for the dynamics of the kEC algorithm in Sec. II of the Supplemental Material [34]. The Fokker-Planck equation contains a term for angular diffusion, a convective term for directed translational motion, and a positional diffusion term, which can be compared with their counterparts in the Fokker-Planck equation for a single ABP. We show that (1) the angular diffusion term agrees in the limit $\langle\Delta t_{\mathrm{EC}}\rangle \ll 1/D_r = \tau$; (2) the convective term agrees with exactly our choice $\langle\Delta \boldsymbol{r}_{\mathrm{EC}}\rangle = \boldsymbol{v}_0\langle\Delta t_{\mathrm{EC}}\rangle$ of the time assignment; and (3) the positional diffusion term agrees in the aforementioned limit $x \to 0$. This is an important result because it establishes a limit where the kEC algorithm becomes exact on the single-particle level. Further inspection of the positional diffusion term in the Fokker-Planck equation shows that we can increase x such that $\ell_{\mathrm{EC}}/\sigma$ becomes of order unity if we are not interested in features of the distribution $P(\boldsymbol{r},\theta,t)$ below one particle diameter σ.

It may be worth noting that the continuous time limit of our algorithm is not affected by the limitations found by Klamser *et al.* [16] mentioned above, mainly because our algorithm does not rely on purely persistent steps by default, as we choose the displacement direction $\boldsymbol{e}_{\mathrm{EC}}$ at the beginning of each EC step randomly.

Additionally, we want to point out that the factor β in Eq. (4), which originates from the rejection mechanism, is indeed the inverse of the thermodynamic temperature. If β would be an arbitrary parameter, this would lead to a Fokker-Planck equation similar to that of an ABP, but with a translational diffusion constant D and a rotational diffusion constant D_r corresponding to different temperatures (according to the Einstein relation), which would not make sense. Added to that, if β was a parameter independent from the inverse temperature, one could simply increase the parameter $\beta \to \infty$ to cause the translational diffusion term to vanish without affecting the temperature.

To recapitulate: For the kEC algorithm to be exact for single ABPs, we require $x \to 0$ and, thus, $\langle\Delta t_{\mathrm{EC}}\rangle \to 0$. Since all physical properties of a system are fixed, the EC length is the only accessible parameter, we can modify, which effectively leads to the condition $\ell_{\mathrm{EC}}/\sigma \to 0$. In reality, we cannot choose arbitrary small displacement lengths without increasing the wall time of the simulation. Nonetheless, reducing ℓ_{EC} will always lead to better results, and we will see that $\ell_{\mathrm{EC}} = 0.01\sigma$ leads to almost exact results, for all types of systems and parameters. A choice $\ell_{\mathrm{EC}} \approx 1\sigma$ is already small enough that deviations in the positional diffusion term of the Fokker-Planck equation should only influence features of the distribution $P_{\mathrm{kEC}}(\boldsymbol{r},\theta,t)$ below one particle diameter σ.

In order to support the claim that the kEC algorithm becomes exact on the level of the probability distribution of a single ABP for $\ell_{\mathrm{EC}}/\sigma \to 0$, we simulate single ABPs in a quadratic box of length $l_{\mathrm{box}} = 8\sigma$ with periodic boundary conditions and measure the one-particle probability density distribution $p_1(\boldsymbol{r},t)$ at $t = 1.5\tau$. We choose $\mathrm{Pe} = 4$ and compare kEC results with a standard Brownian dynamics simulation, which was performed using LAMMPS. Figure 2 reveals that the deviations between both simulation techniques

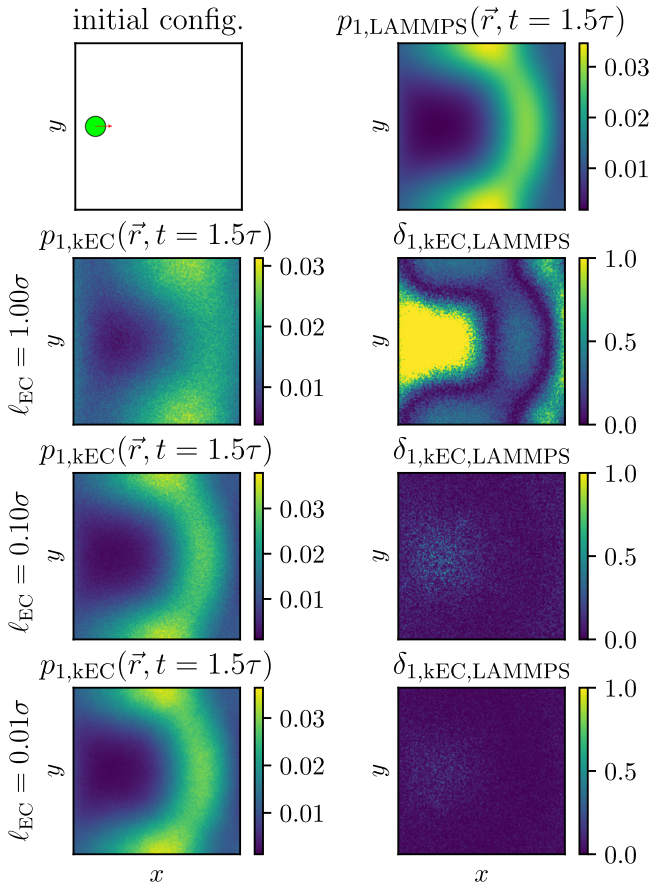

FIG. 2. Probability density distribution $p_1(\boldsymbol{r}, t)$ of a single ABP (Pe = 4) starting from a given initial condition with periodic boundary conditions (see upper left) at $t = 1.5\tau$ using a LAMMPS Brownian dynamics simulation and the kEC algorithm as well as the absolute value of the relative deviation between both algorithms per grid element $\delta_{1,\mathrm{kEC,LAMMPS}} \equiv |(p_{1,\mathrm{kEC}} - p_{1,\mathrm{LAMMPS}})/p_{1,\mathrm{LAMMPS}}|$. The results show an increase in accuracy of the kEC algorithm for decreasing EC length supporting the claim that the kEC algorithm becomes exact in the limit $\ell_{\mathrm{EC}}/\sigma \to 0$.

(right column of Fig. 2) gradually vanish with decreasing EC length ℓ_{EC} from an average absolute value of the relative error per grid element of $\langle \delta_{1,\mathrm{kEC,LAMMPS}}^{\ell_{\mathrm{EC}}=1.00\sigma} \rangle \approx 26.4\%$ ($\beta F_0 \ell_{\mathrm{EC}} = 12$) to just $\langle \delta_{1,\mathrm{kEC,LAMMPS}}^{\ell_{\mathrm{EC}}=0.01\sigma} \rangle \approx 2.3\%$ ($\beta F_0 \ell_{\mathrm{EC}} = 0.12$).

These results are further supported by analyzing the mean square displacement of a single free ABP as a function of time for Pe = 50 in Fig. 3, which shows again that errors decrease for decreasing EC length ℓ_{EC}. This second comparison of a dynamic quantity demonstrates convincingly that the kEC algorithm is not only able to produce almost exact results on short timescales but conveniently also on medium and long timescales.

Even though the two-body problem is the most simple configuration, where interactions between two particles are relevant, we are not able to analytically prove the exactness of our algorithm on the level of a Fokker-Planck equation, which takes collisions into account. However, similar to the one-body problem, we can verify the validity of the kEC algorithm on the two-body level by comparing it to standard simulations of two ABPs in a quadratic box of length $l_{\mathrm{box}} = 6\sigma$ with

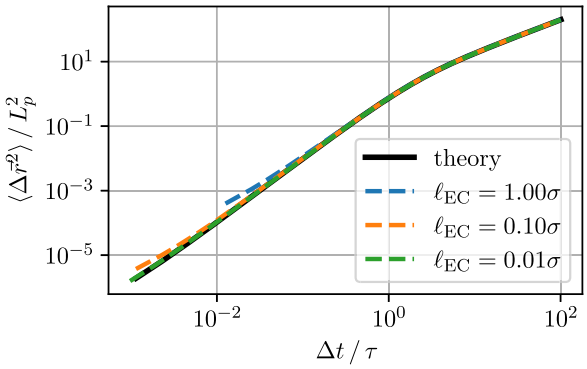

FIG. 3. Comparison between the kEC algorithm and the analytical solution for the mean square displacement $\langle \Delta \boldsymbol{r}^2 \rangle$ of a single free ABP (Pe = 50) as a function of time $\Delta t/\tau$, for different EC lengths ℓ_{EC}. Reducing the EC length improves the accuracy of the algorithm, especially on short timescales.

periodic boundary conditions. We choose the coordinate system in a way that the position of one particle (green) remains fixed and measure the probability density $p_2(\boldsymbol{r}_b, t)$ of the other particle (blue). Here, we compare our results with the EDBD algorithm previously used by Levis *et al.* [24].

In Fig. 4, we show both initial configurations, the probability densities $p_2(\boldsymbol{r}_b, t)$ as well as heatmaps of the absolute value of the relative error per grid element. Regardless of the orientation of the active forces, the Péclet number as well as the time, the average deviation between both simulation techniques shrinks with decreasing EC length just like in the one-body problem. For a more detailed discussion we refer to the Sec. II of the Supplemental Material [34].

As mentioned before, we are not able to analytically verify our algorithm as soon as collisions become relevant. However, we can prove the kEC algorithm to obey the N-body Fokker-Planck equation in the dilute limit $\eta \to 0$ (for the derivation, see Sec. IV of the Supplemental Material [34]). Even though this limit itself is not very interesting, one may argue that the algorithm does not become discontinuously incorrect when the packing fraction is increased to finite values. This theory is supported by the reliability of the kEC algorithm on the two-particle level. Consequently, we anticipate the algorithm to also work correctly for the general many-body case if the event-chain length becomes sufficiently small because ECs involve only two particles in this limit.

Going beyond two particles, we can also test the validity of the many-particle kEC algorithm for static and dynamic quantities. We simulate $N = 5000$ hard ABPs in a quadratic simulation volume of area A and packing fraction $\eta = N\pi\sigma^2/(4A)$. Just like before, the EDBD algorithm serves as the benchmark. We calculate the self-diffusion of ABPs and the probability density $p(\eta_{\mathrm{local}})$ of the local packing fraction η_{local} (for further details see Sec. V A of the Supplemental Material [34]). The probability density $p(\eta_{\mathrm{local}})$ exhibits two peaks if MIPS occurs; positions, heights, and shapes of the peaks provide a very sensitive test of the algorithm. The corresponding results of those measurements are shown in Fig. 5. Comparing both algorithms reveals how relatively large EC lengths, e.g., $\ell_{\mathrm{EC}} = 1.00\sigma$ ($\beta F_0 \ell_{\mathrm{EC}} = 45$–$150$), usually lead to sufficient approximations. In addition, reducing the EC

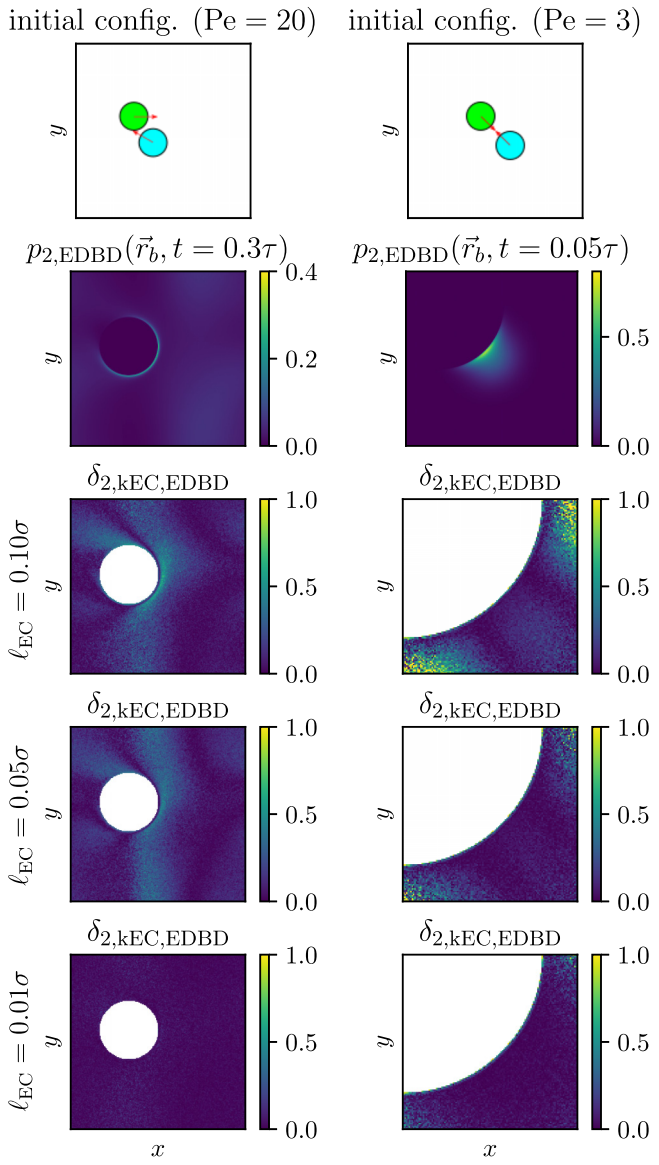

FIG. 4. Probability density distributions $p_2(\boldsymbol{r}_b, t)$ of two hard ABPs using the EDBD algorithm (see second row, using $\tau_B = 0.01$) for two distinct initial configurations (first row) and absolute value of the relative error per grid element $\delta_{2,\mathrm{kEC,EDBD}} \equiv |(p_{2,\mathrm{kEC}} - p_{2,\mathrm{EDBD}})/p_{2,\mathrm{EDBD}}|$ of the kEC algorithm. We choose the coordinate system in a way that the position of the green particle remains fixed and measure the position of the blue particle. The results demonstrate the kEC algorithm's ability to handle interactions and collisions properly if $\ell_{\mathrm{EC}}/\sigma \to 0$.

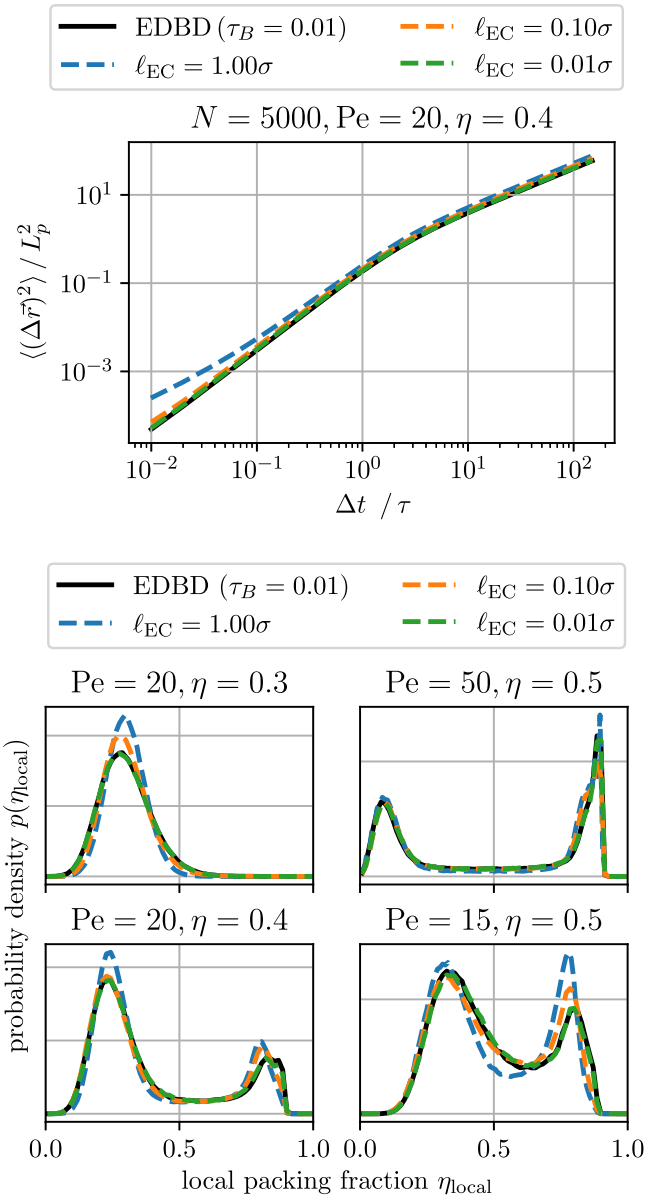

FIG. 5. Comparison of (a) the self-diffusion and (b) probability density of the local packing fraction $p(\eta_{\mathrm{local}})$ for various configurations of hard ABPs using the EDBD algorithm [24] and the kEC algorithm. Using the parameters $\ell_{\mathrm{EC}} = 0.01\sigma$ and $\tau_B = 0.01$, one obtains almost the exact same results.

length—as expected—improves the accuracy of the kEC algorithm to the point where, using $\ell_{\mathrm{EC}} = 0.01\sigma$ ($\beta F_0 \ell_{\mathrm{EC}} = 0.45$–$1.5$), both algorithms produce almost identical results. This holds for different values of the driving force and global packing fraction, regardless of whether MIPS occurs or not.

Concerning the individual simulation time of each particle: If the algorithm would distribute the mean time per EC step falsely, one would definitely expect some deviations for almost every observable and especially the ones that directly depend on time, such as self-diffusion. However, as just presented, the measurement of these very sensitive observables strongly indicates that the limit $\ell_{\mathrm{EC}}/\sigma \to 0$ is conveniently also exact for the many-body problem. The reason for correctness in the limit of short ECs is probably a combination of (1) an increased accuracy of single-particle dynamics, (2) a narrow time distribution (see the Supplemental Material [34]), and (3) a decreasing mean number of particle collisions per ECMC move, effectively leading to two-body interactions, which our algorithm, as previously demonstrated, handles correctly.

IV. MOTILITY-INDUCED PHASE SEPARATION

There are numerous Brownian dynamics simulation studies of MIPS for active soft repulsive disks [10,36–39] or

TABLE I. To quantify the performance of our algorithm on an Intel Xeon W-2245 (8-core, 3.9 GHz), we measure the number of persistence times τ we are able to simulate per day for different packing fractions η and Péclet numbers Pe.

η	Pe	τ/day
0.3	10	∼75 000
0.4	20	∼7000
0.5	40	∼1000
0.6	80	∼200

spheres [38,40], employing Lennard-Jones interactions. However, among all the numerical studies of active particles, results for genuine *hard* disks are actually very rare [23,24,41] and all based on the same EDBD algorithm developed originally for passive hard spheres [22]. As opposed to force-based Langevin or molecular dynamics techniques, the kEC algorithm is particularly suited to study hard particles. We demonstrate the potential of the kEC cluster algorithm to investigate such systems by calculating the MIPS region in the phase diagram of active hard disks. The phase diagram of active hard disks as a function of the packing fraction η in a square system of area A and the Péclet number Pe as well as the extent of the MIPS region also provides another very sensitive test of our kEC algorithm.

Using $\ell_{\mathrm{EC}} = 1.00\sigma$, we can perform simulations of $N = 19\,500$ particles, which are particle numbers that are hard to reach with the EDBD algorithm (Levis *et al.* [24] only simulate $N = 2000$–4000 particles to investigate the phase diagram). Information about typical simulation times of our algorithm on an Intel Xeon W-2245 (8-core, 3.9 GHz) processor are listed in Table I. For a more detailed discussion and a comparison with the EDBD algorithm, see Sec. VI.

Starting from a homogeneous initial packing, we detect whether MIPS occurs (blue points in Fig. 6) and determine the corresponding local coexisting packing fractions (binodal, blue line) from measurements of the probability density $p(\eta_{\mathrm{local}})$ of the local packing fraction η_{local} as exemplified in Fig. 5.

Orange points within the binodal correspond to global packing fractions, where the homogeneous initial state remains metastable, such that the boundary between blue and orange points represents the spinodal line, i.e., the limit of stability of the homogeneous phase (see Sec. V A of the Supplemental Material [34] for more details). The results, using $\ell_{\mathrm{EC}} = 1.00\sigma$, show good agreement with the active hard-disk results of Ref. [24], especially in the region of high activity. Noticeable deviations can only be found in close proximity of the critical point.

To further investigate this, we simulate the region around the critical point for a smaller system of $N = 5000$ particles and smaller values of ℓ_{EC} (see right side of Fig. 6). In accordance with everything mentioned above, we can correct the deviations between the EDBD algorithm and our kEC algorithm by reducing ℓ_{EC}. Finally, the remaining differences that are still present for $\ell_{\mathrm{EC}} = 0.01\sigma$ are almost certainly an artifact of different system sizes being analyzed and, more importantly, different ways of calculating the coexisting densities, relevant for determining the binodal line.

V. ACTIVE PARTICLES WITH SOFT INTERACTIONS

Up to this point, we restricted ourselves to the important case of steric interactions between hard active particles.

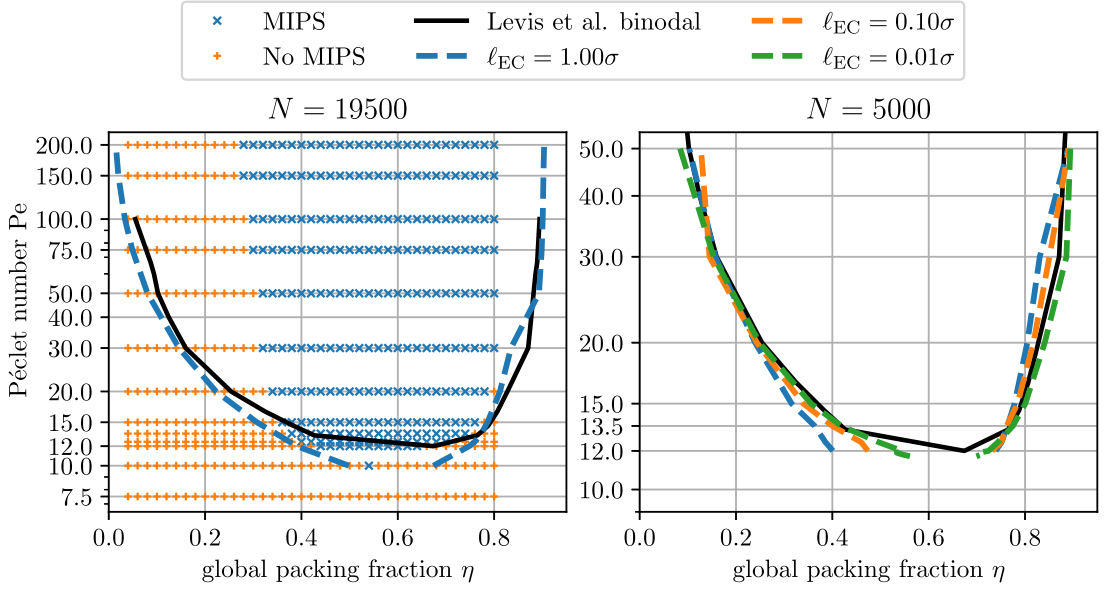

FIG. 6. Left: Phase diagram of active hard disks (kEC: $N = 19\,500$ and area A changing according to the packing fraction η) from kEC simulations using $\ell_{\mathrm{EC}} = 1.00\sigma$. The kEC results for the binodal in general agree with EDBD simulation results ($N = 2000$–4000) of Levis *et al.* [24] except for some deviations around the critical point. Right: Phase diagram of active hard disks (kEC: $N = 5000$) using different values for the EC length. In agreement with the previous observations, reducing ℓ_{EC} leads to better results, especially around the critical point. The remaining deviations are most likely an artifact of different system sizes and ways of calculating the binodal.

Despite this focus, the ECMC algorithm can be extended to include soft interaction energies by generalizing the notion of a rejection and introducing a "virtual" hard-disk radius [26,32]. The question arises whether the kEC algorithm can be extended in a similar way.

The main problem when dealing with soft instead of steric interactions in the kEC algorithm is related to the mean time per EC step. In a many-body simulation of active hard disks, a particle behaves similar to a free particle, apart from the instantaneous collisions. We take advantage of this fact by distributing the time per EC move to all particles contributing to an EC step [see Eq. (7)]. This is no longer true for soft interactions because collisions are not instantaneous anymore. In principle, we have to correct the mean time per EC step by taking the interaction forces into account, which is a highly nontrivial problem. In the following, we will investigate the kEC algorithm's ability to simulate active particles with soft interaction energies without corrections of the mean time per EC as compared to Eq. (7).

As an example system, we consider purely repulsive Weeks-Chandler-Andersen (WCA) particles [42]:

$$V_{\mathrm{WCA}}(r) = \begin{cases} 4\epsilon\left[\left(\frac{\sigma}{r}\right)^{12} - \left(\frac{\sigma}{r}\right)^{6}\right] + \epsilon, & r < \sqrt[6]{2}\sigma, \\ 0, & r \geqslant \sqrt[6]{2}\sigma. \end{cases} \tag{8}$$

In the following, we choose $\epsilon = 100 k_B T$ and measure all lengths in units of σ (i.e., use $\sigma = 1$ effectively) and do not apply any corrections to the mean time per EC step. We simulate $N = 5000$ particles using the kEC algorithm with generalized rejections for different values of the global packing fraction and the Péclet number. To compare and verify our results, we conduct Brownian dynamics simulations using LAMMPS.

Again, we perform measurements of the probability density $p(\eta_{\mathrm{local}})$ of the local packing fraction η_{local} to detect whether MIPS occurs and determine the corresponding local coexisting packing fractions. As Fig. 7 suggests, we obtain fair approximations of the probability densities of the local packing fraction using large EC lengths and very good results by reducing the EC length per step. As for hard disks with the EDBD algorithm, we obtain favorable agreement between the conventional Brownian dynamics algorithm and the kEC algorithm throughout the whole phase diagram for all global packing fractions and Péclet numbers. The only notable deviation of the kEC algorithm to the Brownian dynamics simulation is a slight offset of the low-density, dilute phase peak if MIPS occurs. This is probably a direct consequence of the necessity to alter the mean time per EC step in many-body systems with soft interaction energies.

The example just mentioned proves the applicability of our algorithm to hard-disk-like soft interactions. This feature makes our algorithm stand out: While the EDBD algorithm is only applicable to steric interactions, Brownian dynamics simulations are limited to simulate particles with soft interaction energies, while the kEC algorithm can be used to investigate *both* systems. However, one should keep in mind that without any modifications to $\langle \Delta t_{\mathrm{EC}} \rangle$, we expect deviations to increase, e.g., if the range of the soft pair potential is increased or if its steepness is altered.

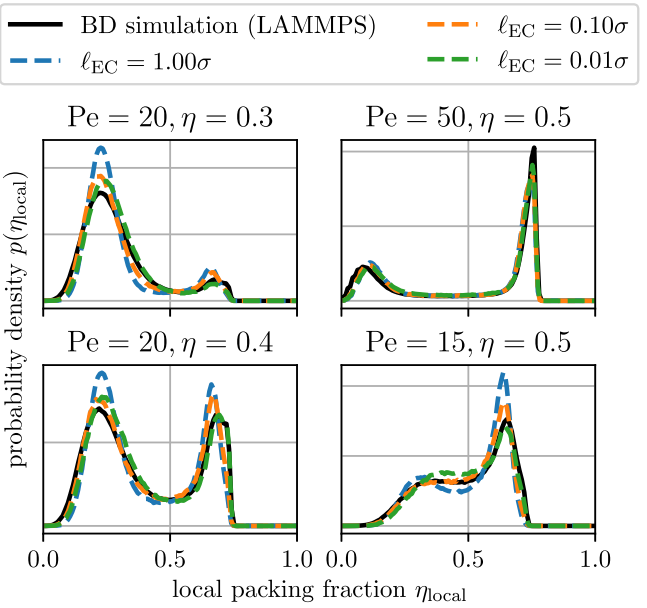

FIG. 7. Comparison of the probability density of the local packing fraction $p(\eta_{\mathrm{local}})$ of WCA particles between the kEC algorithm using different values of the EC length and Brownian dynamics simulations conducted with LAMMPS. Similar to hard-disk-systems, a decrease in ℓ_{EC} generally leads to better agreement with the comparative results.

VI. PERFORMANCE COMPARISON

Algorithms should be both accurate and performant. As mentioned before, the kEC algorithm is able to produce satisfactory approximations as well as exact results, depending on the EC length chosen. Because of the nonlinear relationship between the EC length ℓ_{EC} and the mean time per EC move $\langle \Delta t_{\mathrm{EC}} \rangle$ [see Eq. (6)], the total simulation time increases in the limit $\ell_{\mathrm{EC}}/\sigma \to 0$. However, the EDBD algorithm, which serves as our benchmark for hard disks, suffers from a similar problem: To increase the accuracy, one has to decrease the Brownian time step τ_B [24], which again increases the required simulation time. At this point, it should be emphasized that both algorithms (or rather their frameworks) use sophisticated neighbor lists to reduce the computational effort to detect collisions; e.g., the EDBD algorithm uses a cell list with a complexity of $\mathcal{O}(N)$. However, the EDBD algorithm has another shortcoming. One needs to perform Newtonian dynamics simulations between each time step and avoid possible overlaps by tracking all possible collisions and resolve them in the same order as in a Newtonian dynamics simulation [22].

To demonstrate the performance of our algorithm, we measure the required wall time per persistence time τ of a dense system configuration ($\mathrm{Pe} = 70$ and $\eta = 0.70$, i.e., deep in the MIPS regime) for various system sizes and compare these results with the EDBD algorithm used by Levis *et al.* [24]. For this purpose, we use an Intel Xeon W-2245 (8-core, 3.9 GHz) processor, as before. We proceed in the following way: First of all we focus on the question of which algorithm provides a satisfactory approximation more efficiently, and afterward take a closer look at which algorithm is more performant while producing accurate results.

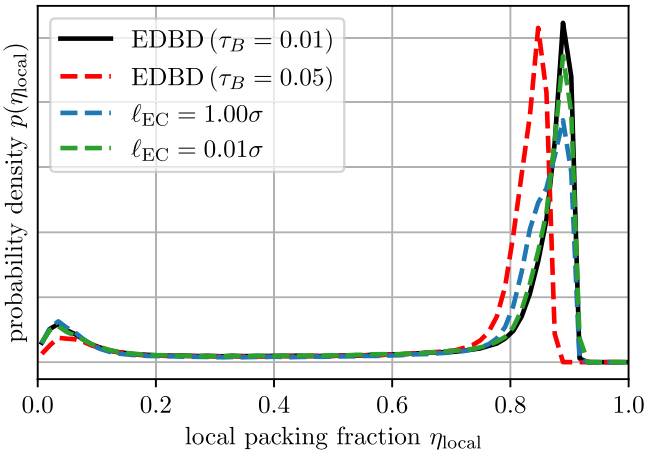

FIG. 8. Probability density of the local packing fraction for a dense configuration (Pe = 70, $\eta = 0.70$, $N = 5000$) of active hard disk using the EDBD and kEC algorithm. Compared to $\tau_B = 0.01$, which serves as a comparative result, $\ell_{EC} = 0.01\sigma$ also leads to exact results. Both $\tau_B = 0.05$ and $\ell_{EC} = 1.00\sigma$ provide good approximations.

Before we can compare both algorithms, we need to find suitable values of ℓ_{EC} and τ_B. For kEC simulations with small EC length $\ell_{EC} = 0.01\sigma$ and EDBD simulations with small Brownian time step $\tau_B = 0.01$, we essentially have agreement of the probability density of the local packing fraction as shown in Fig. 8. Therefore, this can be regarded as the quasiexact result. We choose larger values $\ell_{EC} = 1.00\sigma$ and $\tau_B = 0.05$ to be our simulation parameters for obtaining faster but approximative results also shown in Fig. 8. The only advantage of the EDBD simulation with $\tau_B = 0.05$ compared to kEC with $\ell_{EC} = 1.00\sigma$ is an improved agreement of the shape of the of the probability density for high values of the local packing fraction, but with a non-negligible shift of the high-density peak. In general, the EDBD algorithm with large values of τ_B does not pack the system as densely as it is supposed to be. Apart from this, our algorithm produces far better results in the low-density region as well as the correct position of the high-density peak.

Now, we compare the wall time of the fast but approximative versions of the algorithms with larger values $\ell_{EC} = 1.00\sigma$ and $\tau_B = 0.05$ (see the upper part of Fig. 9). Both algorithms exhibit a power-law dependence on the number of particles N, $\Delta t_{Wall} = aN^k$. An appropriate fit gives exponents $k_{kEC} \approx 1.21$ and $k_{EDBD} \approx 1.99$. The drastically reduced exponent implies a substantial and qualitative performance gain of the kEC algorithm over EDBD simulation for large systems. This performance gain is already realized for relatively small systems with $N \gtrsim 1850$ particles.

We can also compare the wall time of the quasiexact versions of the algorithms with small values $\ell_{EC} = 0.01\sigma$ and $\tau_B = 0.01$ (see the lower part of Fig. 9). Again, we find a power-law dependence on the number of particles N with only slightly smaller exponents $k_{kEC} \approx 1.17$ and $k_{EDBD} \approx 1.93$. Therefore, the kEC algorithm also proves to be qualitatively superior regarding the overall computation time when it comes to providing exact result for large systems. For the chosen parameter values deep in the MIPS phase, the kEC algorithm is already faster for $N \gtrsim 500$ particles.

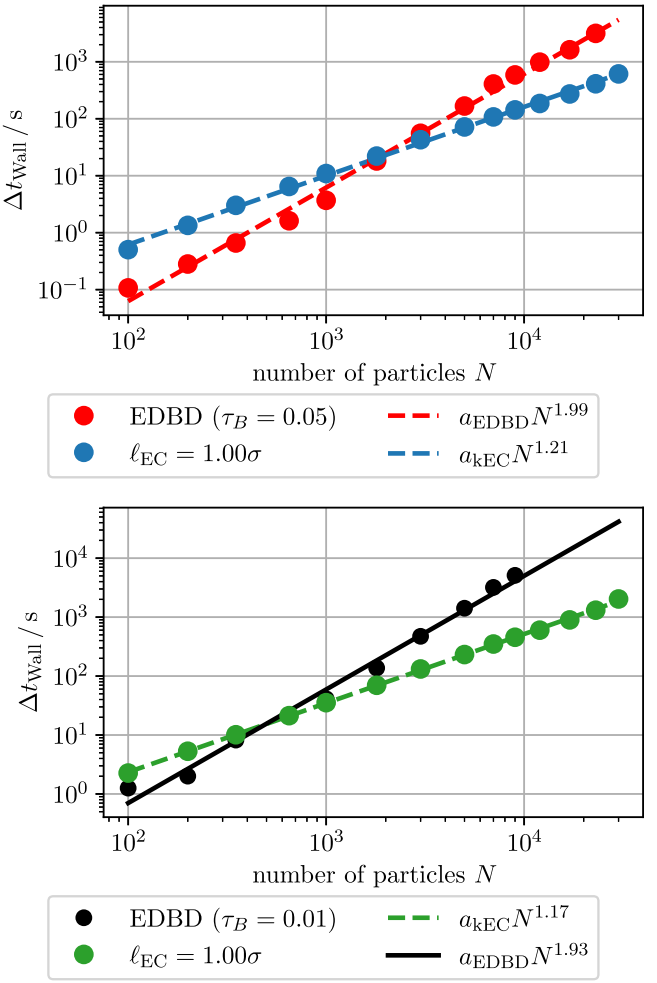

FIG. 9. Upper: Performance comparison between the kEC algorithm ($\ell_{EC} = 1.00\sigma$) and the EDBD algorithm ($\tau_B = 0.05$) used by Levis *et al.* [24] for a dense configuration (Pe = 70, $\eta = 0.70$), with special focus on producing satisfactory approximations. Lower: Performance comparison between the kEC algorithm ($\ell_{EC} = 0.01\sigma$) and the EDBD algorithm ($\tau_B = 0.01$) with special focus on producing exact results. As the data suggests, the kEC algorithm is the superior algorithm regarding both comparisons when it comes to simulating dense systems of active particles efficiently.

Since both algorithms use neighbor list, as mentioned before, the process of tracking and resolving collisions takes (as expected) a toll on the computational complexity of the EDBD algorithm. Consequently, regarding both comparisons, we expect the efficiency advantage of our algorithm to improve even further, the denser the entire system and the denser the liquid phase gets if MIPS occurs, as the number of collisions per time step will increase in dense regions.

VII. GIANT SYSTEM SIZES

As demonstrated and quantified in the previous section, the performance of our algorithm is superior to the EDBD algorithm for large and dense systems of ABPs. Therefore, the kEC algorithm opens up the possibility to study the two most

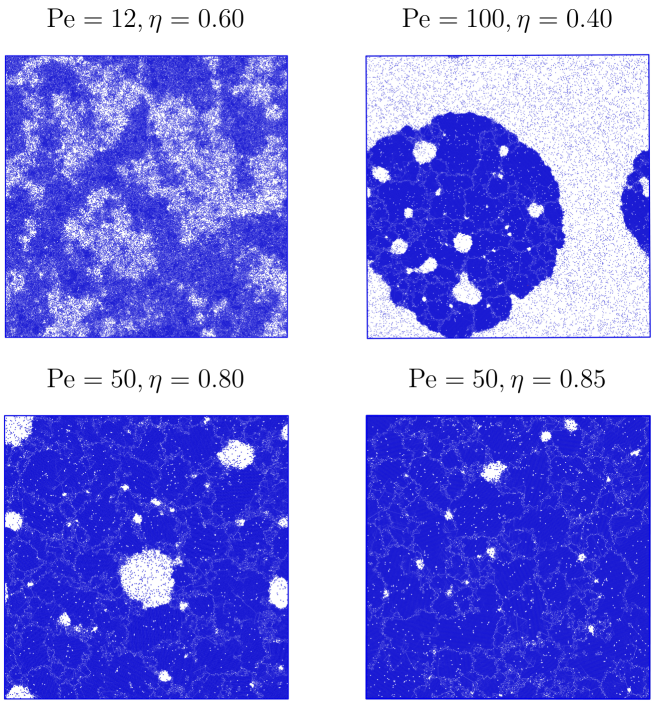

FIG. 10. Exemplary snapshots of various configurations, each consisting of $N = 10^5$ particles. Upper left: System close to the critical point. Upper right: Formation of MIPS at high Péclet numbers. Lower row: High-density regime of the phase diagram. The emergence of small gas bubbles with various lifetimes within dense clusters is in agreement with observations made in Ref. [43].

interesting regions of the phase diagram, namely, the critical point and the high-density regime, using large or even giant system sizes to reduce finite-size effects. Figure 10 shows exemplary snapshots for a system containing $N = 10^5$ particles for various parameter values in different regions of the phase diagram. All examples have reached their characteristic stationary state behavior using the kEC simulation technique.

VIII. DISCUSSION

We introduced a kinetic cluster MC algorithm for active systems, the kEC algorithm to simulate active hard disks. To our knowledge, this is the first kinetic MC algorithm moving entire clusters of particles (in form of ECs) in order to achieve high numerical performance. The basic idea is to distribute a mean time $\langle \Delta t_{\mathrm{EC}} \rangle$, which is analytically calculated for a single particle, among all particles participating in a cluster EC move under the action of the active forces and to use this mean time to rotate active forces diffusive after each cluster move. This establishes a mapping onto ABPs. Our rule to distribute the mean time yields constant currents along a moved EC, thus making the algorithm suitable to explore stationary states of this nonequilibrium system. The concept of cluster moves in a kinetic MC algorithm inevitably leads to the concept of an "individual simulation time" for each particle within this class of algorithms. If we decrease activity to zero (and consider the limit of vanishing Péclet number $\mathrm{Pe} \to 0$), we essentially endow the ECMC algorithm for passive hard disks or spheres with an individual simulation time, which makes dynamical properties such as self-diffusion behavior accessible to ECMC simulations. We can show that for the active (and passive) hard-disk system the distribution of individual simulation times remains sufficiently narrow to warrant correct results.

We analyzed different observables, both of static and of dynamic nature, for various one-, two-, and many-body systems of active hard disks, as well as the phase diagram with special focus on the MIPS region. For all of these quantities, performance and accuracy of the kEC algorithm can be tuned via the EC length parameter ℓ_{EC}: We are able to produce good approximations in fast simulations for $\ell_{\mathrm{EC}} \approx 1\sigma$ and exact results in the limit $\ell_{\mathrm{EC}}/\sigma \to 0$. We can rigorously prove the algorithm to be exact in this limit for the one-body problem and dilute N-body systems, as our algorithm correctly reproduces the corresponding Fokker-Planck equations. We performed extensive numerical checks that the kEC algorithm is exact also on the two- and many-body level, but are lacking an analytical proof, which we have to leave for future research.

In addition, we successfully demonstrated the possibility to apply our method to soft particles by simulating purely repulsive active WCA particles, whose interaction forces only become relevant if the particles come very close. A generalization to arbitrary soft interactions will require to adjust the mean time per EC move by taking the effect of interaction forces into account, which leads to nontrivial "collisions" of nonzero duration. Nevertheless, this makes our algorithm stand out among other simulation techniques, as it would be possible to simulate steric and soft interactions, whereas other methods like an event-driven approach or a Brownian dynamics simulation are only able to handle one interaction type.

Finally, regarding active hard disks, a performance comparison revealed the kEC algorithm to be superior to the EDBD algorithm (at comparable accuracy). This performance gain is substantial for large systems as simulation times scale with significantly lower exponents with the number of particles. This allows us to simulate large and dense systems of ABPs much more efficiently and may open the way for a more effective simulation of other active systems if the method can be generalized. With the kEC algorithm, giant simulations with 10^5 active hard disks become possible on standard desktop hardware.

Since the ECMC method—the basis for our algorithm—is applicable across a wide range of physical problems, we expect that with minor modifications the kEC algorithm can be extended to more complex active systems. Potential applications include polydisperse mixtures of active and passive particles (relevant for studying phenomena such as active depletion forces or enhanced diffusion of passive tracers), the aforementioned generalization to arbitrary soft interactions, and the addition of external forces or other objects, such as polymers. Importantly, our method is not limited to two dimensions, as the core ideas can be readily extended to three-dimensional simulations. Preliminary work on polydisperse mixtures of active and passive particles shows that additional challenges arise: The concept of an "individual simulation time" is harder to handle in this case, as active and passive particles tend to develop distinct time distributions, which can cause difficulties, in particular, for dynamic observables.

ACKNOWLEDGMENTS

The authors are grateful to Demian Levis for providing the code of the Event-Driven Brownian-Dynamics simulation framework. T.A.K. acknowledges financial support by the Deutsche Forschungsgemeinschaft (DFG, German Research Foundation) (Grant No. 4897/1–1).

J.K. and T.A.K. conceived the project. N.S., T.S., and T.A.K. designed the simulations, which were performed and analyzed by N.S. and T.S. The theoretical analysis was conducted by N.S. and J.K. The manuscript was written and revised by N.S. and J.K. with help of T.S. and T.A.K.

DATA AVAILABILITY

The simulation code and data for the kEC algorithm, as well as the analysis code, is openly available in Ref. [44]. All data generated with this code and presented in the Figures are available upon reasonable request from the authors.

[1] R. Bebon, J. F. Robinson, and T. Speck, Thermodynamics of active matter: Tracking dissipation across scales, Phys. Rev. X **15**, 021050 (2025).

[2] M. C. Marchetti, J. F. Joanny, S. Ramaswamy, T. B. Liverpool, J. Prost, M. Rao, and R. A. Simha, Hydrodynamics of soft active matter, Rev. Mod. Phys. **85**, 1143 (2013).

[3] C. Bechinger, R. Di Leonardo, H. Löwen, C. Reichhardt, G. Volpe, and G. Volpe, Active particles in complex and crowded environments, Rev. Mod. Phys. **88**, 045006 (2016).

[4] J. Elgeti, R. G. Winkler, and G. Gompper, Physics of microswimmers—Single particle motion and collective behavior: A review, Rep. Prog. Phys. **78**, 056601 (2015).

[5] T. Surrey, F. Nedelec, S. Leibler, and E. Karsenti, Physical properties determining self-organization of motors and microtubules, Science **292**, 1167 (2001).

[6] K. Kruse, J. F. Joanny, F. Jülicher, J. Prost, and K. Sekimoto, Asters, vortices, and rotating spirals in active gels of polar filaments, Phys. Rev. Lett. **92**, 078101 (2004).

[7] P. Kraikivski, R. Lipowsky, and J. Kierfeld, Enhanced ordering of interacting filaments by molecular motors, Phys. Rev. Lett. **96**, 258103 (2006).

[8] X.-L. Wu and A. Libchaber, Particle diffusion in a quasi-two-dimensional bacterial bath, Phys. Rev. Lett. **84**, 3017 (2000).

[9] T. Vicsek and A. Zafeiris, Collective motion, Phys. Rep. **517**, 71 (2012).

[10] J. Bialké, H. Löwen, and T. Speck, Microscopic theory for the phase separation of self-propelled repulsive disks, Europhys. Lett. **103**, 30008 (2013).

[11] M. E. Cates and J. Tailleur, Motility-induced phase separation, Annu. Rev. Condens. Matter Phys. **6**, 219 (2015).

[12] M. R. Shaebani, A. Wysocki, R. G. Winkler, G. Gompper, and H. Rieger, Computational models for active matter, Nat. Rev. Phys. **2**, 181 (2020).

[13] D. Levis and L. Berthier, Clustering and heterogeneous dynamics in a kinetic Monte Carlo model of self-propelled hard disks, Phys. Rev. E **89**, 062301 (2014).

[14] J. U. Klamser, S. C. Kapfer, and W. Krauth, Thermodynamic phases in two-dimensional active matter, Nat. Commun. **9**, 5045 (2018).

[15] J. U. Klamser, S. C. Kapfer, and W. Krauth, A kinetic-Monte Carlo perspective on active matter, J. Chem. Phys. **150**, 144113 (2019).

[16] J. U. Klamser, O. Dauchot, and J. Tailleur, Kinetic Monte Carlo algorithms for active matter systems, Phys. Rev. Lett. **127**, 150602 (2021).

[17] R. H. Swendsen and J.-S. Wang, Nonuniversal critical dynamics in Monte Carlo simulations, Phys. Rev. Lett. **58**, 86 (1987).

[18] U. Wolff, Collective Monte Carlo updating for spin systems, Phys. Rev. Lett. **62**, 361 (1989).

[19] E. P. Bernard, W. Krauth, and D. B. Wilson, Event-chain Monte Carlo algorithms for hard-sphere systems, Phys. Rev. E **80**, 056704 (2009).

[20] A. Stukowski, Visualization and analysis of atomistic simulation data with OVITO-The open visualization tool, Modell. Simul. Mater. Sci. Eng. **18**, 015012 (2010).

[21] A. P. Thompson, H. M. Aktulga, R. Berger, D. S. Bolintineanu, W. M. Brown, P. S. Crozier, P. J. in 't Veld, A. Kohlmeyer, S. G. Moore, T. D. Nguyen, R. Shan, M. J. Stevens, J. Tranchida, C. Trott, and S. J. Plimpton, LAMMPS—A flexible simulation tool for particle-based materials modeling at the atomic, meso, and continuum scales, Comput. Phys. Commun. **271**, 108171 (2022).

[22] A. Scala, T. Voigtmann, and C. De Michele, Event-driven Brownian dynamics for hard spheres, J. Chem. Phys. **126**, 134109 (2007).

[23] R. Ni, M. A. Stuart, and M. Dijkstra, Pushing the glass transition towards random close packing using self-propelled hard spheres, Nat. Commun. **4**, 2704 (2013).

[24] D. Levis, J. Codina, and I. Pagonabarraga, Active Brownian equation of state: Metastability and phase coexistence, Soft Matter **13**, 8113 (2017).

[25] W. Krauth, Event-chain Monte Carlo: Foundations, applications, and prospects, Front. Phys. **9**, 663457 (2021).

[26] M. Michel, S. C. Kapfer, and W. Krauth, Generalized event-chain Monte Carlo: Constructing rejection-free global-balance algorithms from infinitesimal steps, J. Chem. Phys. **140**, 054116 (2014).

[27] M. Michel, J. Mayer, and W. Krauth, Event-chain Monte Carlo for classical continuous spin models, Europhys. Lett. **112**, 20003 (2015).

[28] T. A. Kampmann, H.-H. Boltz, and J. Kierfeld, Monte Carlo simulation of dense polymer melts using event chain algorithms, J. Chem. Phys. **143**, 044105 (2015).

[29] Y. Nishikawa and K. Hukushima, Event-chain Monte Carlo algorithm for continuous spin systems and its application, J. Phys.: Conf. Ser. **750**, 012014 (2016).

[30] J. Harland, M. Michel, T. A. Kampmann, and J. Kierfeld, Event-chain Monte Carlo algorithms for three-and many-particle interactions, Europhys. Lett. **117**, 30001 (2017).

[31] M. Klement and M. Engel, Efficient equilibration of hard spheres with Newtonian event chains, J. Chem. Phys. **150**, 174108 (2019).

[32] T. A. Kampmann, D. Müller, L. P. Weise, C. F. Vorsmann, and J. Kierfeld, Event-chain Monte-Carlo simulations

of dense soft matter systems, Front. Phys. **9**, 635886 (2021).

[33] N. Metropolis, A. W. Rosenbluth, M. N. Rosenbluth, A. H. Teller, and E. Teller, Equation of state calculations by fast computing machines, J. Chem. Phys. **21**, 1087 (1953).

[34] See Supplemental Material at http://link.aps.org/supplemental/10.1103/hhbb-ph5s for details on the kEC algorithm, its validity, the derivation of the Fokker-Planck equation, a discussion about the time distribution, and simulations for the phase diagram of hard disks.

[35] R. K. P. Zia and B. Schmittmann, Probability currents as principal characteristics in the statistical mechanics of non-equilibrium steady states, J. Stat. Mech. (2007) P07012.

[36] Y. Fily and M. C. Marchetti, Athermal phase separation of self-propelled particles with no alignment, Phys. Rev. Lett. **108**, 235702 (2012).

[37] G. S. Redner, M. F. Hagan, and A. Baskaran, Structure and dynamics of a phase-separating active colloidal fluid, Phys. Rev. Lett. **110**, 055701 (2013).

[38] J. Stenhammar, D. Marenduzzo, R. J. Allen, and M. E. Cates, Phase behaviour of active Brownian particles: The role of dimensionality, Soft Matter **10**, 1489 (2014).

[39] J. Martin-Roca, R. Martinez, L. C. Alexander, A. L. Diez, D. G. A. L. Aarts, F. Alarcon, J. Ramírez, and C. Valeriani, Characterization of MIPS in a suspension of repulsive active Brownian particles through dynamical features, J. Chem. Phys. **154**, 164901 (2021).

[40] A. Wysocki, R. G. Winkler, and G. Gompper, Cooperative motion of active Brownian spheres in three-dimensional dense suspensions, Europhys. Lett. **105**, 48004 (2014).

[41] N. de Macedo Biniossek, H. Löwen, T. Voigtmann, and F. Smallenburg, Static structure of active Brownian hard disks, J. Phys.: Condens. Matter **30**, 074001 (2018).

[42] J. D. Weeks, D. Chandler, and H. C. Andersen, Role of repulsive forces in determining the equilibrium structure of simple liquids, J. Chem. Phys. **54**, 5237 (1971).

[43] C. B. Caporusso, P. Digregorio, D. Levis, L. F. Cugliandolo, and G. Gonnella, Motility-induced microphase and macrophase separation in a two-dimensional active Brownian particle system, Phys. Rev. Lett. **125**, 178004 (2020).

[44] N. Schaffrath, T. Sathiyanesan, T. A. Kampmann, and J. Kierfeld, Kinetic event-chain algorithm for active matter, TU Dortmund Gitlab (2026), https://gitlab.tu-dortmund.de/cmt/kierfeld/kinetic-event-chain-algorithm-for-active-matter/-/tree/1a4436345f8eedbf4e291ff3ddaf422610fac8e5/.